APPLICATION OF RPI MODEL: PREDICTION OF SUBCOOLED BOILING AND DNB IN VERTICAL PIPES

Rui Zhang, Wenwen Zhang, Tenglong Cong, Wenxi Tian, G H Su, Suizheng Qiu
School of Nuclear Science and Technology, Xi'an Jiaotong University, Xi'an, China
Email: ruizhang@stu.xjtu.edu.cn

ABSTRACT

In this work, the RPI wall boiling model is used to predict the subcooled boiling for water and Freon and the CHF for water in vertical pipes. The heat flux is divided into four parts in the RPI wall boiling model, i.e., evaporation heat flux, convective heat flux and quench heat flux for liquid phase and the convective heat flux for vapor phase. The wetted fraction of each phase is correlated by an empirical correlation. In the subcooled boiling applications, the calculated wall temperature, fluid temperature and void fraction distribution are compared with the experiment data. In the CHF applications, the predicted CHFs are compared with experimental values. The deviation of the CHF values are less than 15% when compared to experiment data, which is much better than empirical correlations. Besides, the parameter analysis is performed to investigate the effects of L/D, D, inlet subcooling and pressure on CHF.

KEYWORDS
RPI; CHF; subcooled boiling

1. INTRODUCTION

Subcooled boiling denotes the physical phenomenon where the wall temperature is high enough to motivate boiling at the wall even though the bulk average temperature is below the saturation value. More and more attention has been attracted by subcooled boiling for its great improvement on the capacity of heat transfer for pipes compared with single phase forced convection. However, heat transfer ability can not always be enhanced by subcooled boiling with increasing wall heat flux, since heat transfer deterioration may occur when heat flux reach a certain value, named critical heat flux (CHF). CHF refers to the heat transfer limit causing a sudden decrease in the heat transfer coefficient and possible failure of facility in which evaporation or boiling is occurring. In the past decades, CHF was investigated by experiments and empirical or semi-empirical correlations developed based on experiments in general. However, the usage of all these experiments and correlations was limited by application scope, i.e., range of experiment data. Besides, correlations can be used only for a certain geometry since the experiments were executed in corresponding geometry.

In this paper, a commercial CFD code Fluent was adapted for predicting the subcooled boiling flow in a single pipe under both high pressure and low pressure. The Eulerian two-phase model exactly considering the inter-phase exchange was used. By comparing with experiment, the simulated local flow characteristics were analyzed and discussed. Moreover, CHF model based on RPI wall boiling model was employed to study the DNB phenomena and to predict CHF in vertical pipes. The calculated CHF data were compared with experiment data of Celata et al [1] to validate the CHF model. The comparison between calculated and experimental CHF data shows that the CHF model has potential to predict the CHF in fuel assembly.

2. PHYSICAL MODEL

Eulerian multiphase model as well as interphase mass, momentum and energy transfer models is employed to consider the non-equilibrium between two phases. All these interphase interactions are calculated based on the interfacial area density model. Subcooled boiling at wall is modeled by the RPI wall boiling model proposed by Kurual and Podowski[2]. The liquid phase is treated as a continuous phase while vapor phase as dispersed phase. Whereas CHF mechanism is modeled by the improved wall boiling model (i.e., the CHF model). The governing equations and auxiliary equations are given in the following of this part.

2.1 Conservation Equation

Conservation equations of Eulerian two-phase model include mass, momentum and energy equations for each phase, i.e.,
mass equation

$$\frac{\partial}{\partial t}\left(\alpha_i \rho_i\right)+\nabla\cdot\left(\alpha_i \rho_i \vec{v}_i\right)=S_i+\dot{m}_{ji}-\dot{m}_{ij} \tag{1}$$

momentum equation

$$\begin{aligned}&\frac{\partial\left(\alpha_i \rho_i \vec{v}_i\right)}{\partial t}+\nabla\cdot\left(\alpha_i \rho_i \vec{v}_i \vec{v}_i\right)=-\alpha_i \nabla p+\nabla\cdot\bar{\bar{\tau}}_i+\alpha_i \rho_i \vec{g}\\&+\dot{m}_{ji}\vec{v}_j-\dot{m}_{ij}\vec{v}_i+\vec{F}_{D,i}+\vec{F}_{L,i}+\vec{F}_{wl,i}+\vec{F}_{td,i}+\vec{F}_{vm,i}\end{aligned} \tag{2}$$

energy equation

$$\frac{\partial}{\partial t}\left(\alpha_i \rho_i h_i\right)+\nabla\cdot\left(\alpha_i \rho_i \vec{v}_i h_i\right)=\alpha_i \frac{\partial p_i}{\partial t}-\nabla\cdot\vec{q}_i+S_i+Q_{ij}+\dot{m}_{ji}h_j-\dot{m}_{ij}h_i \tag{3}$$

where α_i, ρ_i, $\vec{v}_i$, S_i, p_i, $\bar{\bar{\tau}}_i$, h_i and $\vec{q}_i$ denote the volume of fraction, density, velocity, source term, pressure, stress tensor, specific enthalpy and heat flux for *i* phase, respectively. $\dot{m}_{ji}$ and Q_{ji} are the mass and energy transfer from *j*th to *i*th phase, separately. $\vec{F}_{D,i}$, $\vec{F}_{L,i}$, $\vec{F}_{wl,i}$, $\vec{F}_{td,i}$ and $\vec{F}_{vm,i}$ are the drag force, lift force, wall lubrication force, turbulence dispersion force and virtual mass force, respectively.

2.2 Wall Boiling Model

According to RPI wall boiling model proposed by Kurul and Podowski[2], the total heat flux from heated wall to the fluid is partitioned into three components, the single-phase convective heat flux q_C, the evaporate heat flux q_E and the wall quenching heat flux q_Q, i.e.,

$$q_W=q_C+q_E+q_Q \tag{4}$$

These three heat fluxes can be expressed as,

$$q_C=h_C\left(T_w-T_l\right)\left(1-A_b\right) \tag{5}$$

$$q_E=V_d N_w \rho_g h_{fg} f \tag{6}$$

$$q_Q=\frac{2\sqrt{k_l \rho_l c_{p,l} f}}{\sqrt{\pi}}\left(T_w-T_l\right) \tag{7}$$

where h_C denotes the single phase turbulent heat transfer coefficient which depends on the velocity profile and is calculated using turbulent wall temperature function; T_w and T_l are the wall and fluid temperatures, respectively; ρ_l and ρ_g are the density of liquid and vapor phase, respectively; h_{fg} is the latent heat of evaporation; V_d is the volume of the

bubbles based on the bubble departure diameter; $c_{p,l}$ and k_l are the specific heat and conductivity of liquid phase, respectively. A_b is the proportion of heated wall covered by nucleating bubbles, estimated by

$$A_b = \min\left(1, K\frac{N_w \pi d_{bw}^2}{4}\right) \tag{8}$$

where d_{bw} is the bubble departure diameter, given by Tolubinsky model[3],

$$d_{bw} = \min\left(0.0006 \cdot e^{\left(-\frac{\Delta T_{sub}}{45.0}\right)}, 0.0014\right) \tag{9}$$

and K is an empirical constant estimated by Del Valle and Kenning equation[4]

$$K = 4.8\exp\left(-\frac{\rho_l c_{p,l}\left(T_w - T_l\right)}{80\rho_g h_{fg}}\right) \tag{10}$$

N_w is the active nucleate site density, given by Lemmert and Chawla[5] model

$$N_w = 210^{1.805}\left(T_w - T_{sat}\right)^{1.805} \tag{11}$$

where T_{sat} is the saturated temperature. f is the frequency of bubble departure, given by Cole correlation [6],

$$f = \frac{1}{T} = \sqrt{\frac{4g(\rho_l - \rho_g)}{3d_{bw}\rho_l}} \tag{12}$$

where g is the gravitational acceleration.

2.3 CHF Model

For CHF model employed in this work, the total heat flux from heated wall to the fluid is divided into two components, heat flux transferred to liquid phase (q_f) and heat flux transferred to vapor phase (q_g). Among these two components, heat flux to liquid phase is partitioned into three parts, which has the same specification as previous RPI wall boiling model. Thus, the total heat flux can be expressed as

$$q_w = f\left(\alpha_f\right)\left(q_c + q_e + q_q\right) + \left(1 - f\left(\alpha_f\right)\right)q_g \tag{13}$$

where $f\left(\alpha_f\right)$ is the area fraction of heated wall dominated by liquid phase, including the wall area fractions covered by convective liquid phase and by nucleating bubbles; $\left(1 - f\left(\alpha_f\right)\right)$ is the area fraction of heated wall covered by single phase vapor; $f\left(\alpha_f\right)$ is estimated by Tentner model [7]

$$f(\alpha_g) = 1 - f(\alpha_f) = \begin{cases} 0 & \alpha_g < \alpha_{g,1} \\ \frac{1}{2}\left(1 - \cos\left(\pi\frac{\alpha_g - \alpha_{g,1}}{\alpha_{g,2} - \alpha_{g,1}}\right)\right) & \alpha_{g,1} \le \alpha_g \le \alpha_{g,2} \\ 1 & \alpha_g > \alpha_{g,2} \end{cases} \tag{14}$$

where the breakpoints have been set to $\alpha_{g,1} = 0.9$ and $\alpha_{g,2} = 0.95$.

The heat flux transferred to vapor phase can be expressed as,

$$q_g = h_g(T_w - T_g) \tag{15}$$

where h_g denotes the single phase turbulent heat transfer coefficient of vapor phase; T_w and T_g are the temperature of heated wall, liquid and fluid, respectively

2.4 Interfacial Heat Transfer

Interfacial heat transfer includes the heat transfer from liquid to vapor phase at the near wall region and the heat transfer between vapor and liquid phases in the subcooled bulk. Heat transferred to vapor is calculated by

$$\dot{q}_{vt} = \frac{\alpha_v \rho_v C_{p,v}}{\delta t}(T_{sat} - T_v) \tag{16}$$

where δt is the time scale set to a default value of 0.05 according to [8].

When the bubble departs from the heated wall and moves towards the subcooled mainstream, the heat transferred from the vapor to the liquid is calculated as,

$$\dot{q}_{lt} = h_{sl}(T_{sat} - T_l) \tag{17}$$

where h_{sl} is the volumetric heat transfer coefficient calculated by Ranz-Marshall model[9].

2.5 Interfacial Mass Transfer

For subcooled boiling, the process of mass transfer consists of these two aspects: liquid evaporation near the wall and liquid evaporation or vapor condensation in bulk flow. The evaporation mass flux in near wall cells can be calculated on the basis of evaporation heat flux,

$$\dot{m}_E = \frac{\dot{q}_E}{h_{fg} + C_{p,l}\Delta T_{sub}} \tag{18}$$

Mass transfer rate in subcooled region depends on the difference of temperature between each phase. When the liquid is subcooled, steam condensates; when the liquid is superheated, liquid evaporates. The interfacial mass transfer rate can be written as,

$$\dot{m} = \dot{m}_{lt} + \dot{m}_{vt} = \frac{\dot{q}_{lt} + \dot{q}_{vt}}{h_{fg}} \tag{19}$$

2.6 Interfacial Momentum Transfer

The interfacial momentum transfer between liquid and vapor phases includes the drag force, lift force, wall lubrication force and turbulent dispersion force, which are given in detail.

The drag force, which is flow region dependent, is modeled by

$$F_D = \frac{C_D \mu_l A_{if} \,\mathrm{Re}}{8 d_g}\left(\vec{v}_g - \vec{v}_l\right) \tag{20}$$

where C_D is the drag force coefficient, estimated by Ishii model [10]; μ_l is the viscosity of liquid phase; A_{if} is the interfacial area concentration; Re is the relative Reynolds number based on the average bubble diameter; d_g is the average bubble diameter.

The lift force, presenting the force act on vapor phase due to velocity gradients in the liquid phase, is calculated by

$$\vec{F}_L = -C_L \rho_l \alpha_g \left(\vec{v}_l - \vec{v}_g\right) \times \left(\nabla \times \vec{v}_l\right) \tag{21}$$

where C_L is the lift force coefficient given by Moraga model[11].

The wall lubrication force, used to push the vapor phase away from the walls to bulk flow, is defined as

$$\vec{F}_{wl} = C_{wl} \rho_l \alpha_g \left|\vec{v}_{l,z} - \vec{v}_{g,z}\right|^2 \vec{n}_w \tag{22}$$

where C_{wl} is the wall lubrication coefficient given by Antal model[12]; $\vec{v}_{l,z}$ and $\vec{v}_{g,z}$ are the velocity component tangential to the wall surface of liquid and vapor phase, respectively;

$\vec{n}_w$ is the unit normal pointing away from the wall.

The turbulent dispersion force, including the effects of interphase turbulent momentum transfer, play a key role in take the vapor away from the near wall region to the subcooled bulk. It can be calculated by Burns model[13],

$$\vec{F}_{td} = C_{TD} \frac{C_D \mu_l \mu_{t,l} A_{if} \ \mathrm{Re}}{8 d_g \rho_l \sigma_{lg}} \left(\frac{\nabla \alpha_g}{\alpha_g} - \frac{\nabla \alpha_l}{\alpha_l} \right) \tag{23}$$

where $C_{TD} = 1$ and $\sigma_{\mathrm{lg}} = 0.9$.

Interfacial area concentration is a key parameter for predicting mass, momentum and energy transfer through the interface between phases. When using the Eulerian multiphase model, the default interfacial area concentration is an algebraic relationship between a specific bubble diameter and the interfacial area concentration.

$$A_i = \frac{6 \alpha_p (1 - \alpha_p)}{d_p} \tag{24}$$

where the volume fraction α_p is for a dispersed phase p.

2.7 Turbulence model

After comparing calculated results with experimental data of subcooled boiling and CHF, realizable k-ε turbulence model and enhanced wall function were employed to solve the turbulent parameters.

3. SUBCOOLED BOILING PREDICTION

The experiment is conducted in a 2 m long pipe with a uniform wall heat flux with diameter of 15.4mm. The heat flux of the test section is 5.7×10^5 W/m^2 and the inlet boundary is given as mass flow inlet boundary with mass flow rate of 900 kg/(m^2 s) and inlet subcooling of 58.2K, as **Figure** 1a shows. The RPI boiling model with corresponding closure models as mentioned before is employed in this simulation. The numerical simulation results are in good accordance with measured data, as shown in **Figure** 1(b).

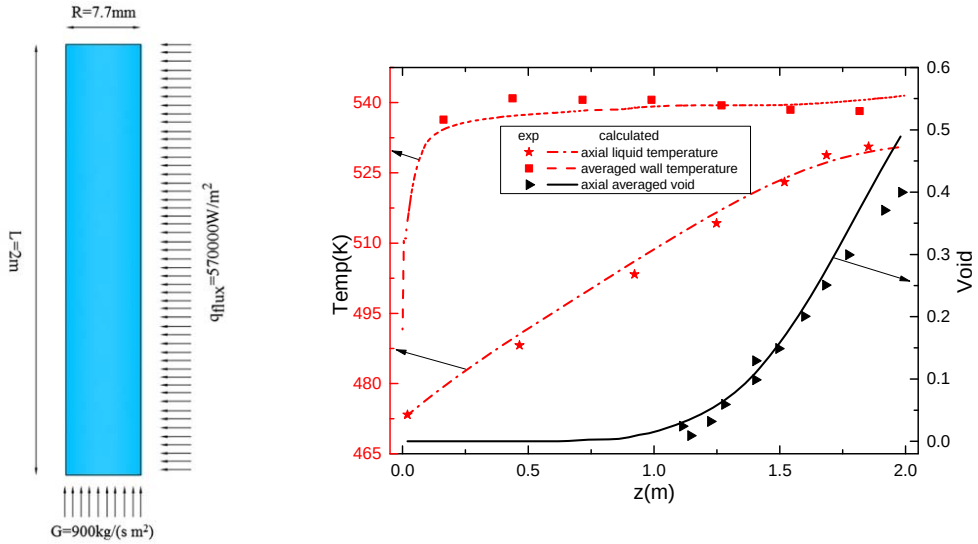

(a) geometry and boundary conditions (b) Comparison of measured (symbols) and calculated(lines) averaged void, liquid temperature and wall temperature

Figure 1 calculated profile and experiment test

To substantiate the reliability of RPI wall boiling model, numerical simulation of experiments published by Bartolomei (1982) [14] were conducted. The test section is made of Cr18Ni10Ti steel, and is 12mm in diameter. The length of heated tube is from 800 to 1500mm, and uniform heat flux density is given at the tube wall. The range of experiment parameters was: in regard to pressure 3-15MPa, in regard to heat flux 0.4-2.5MPa, and in regard to mass velocity 400-3000kg/m^2·s. The experiment results give the true volumetric vapor content over the length. The simulation is performed in a vertical pipe similar to the experiment. The boundary conditions can be explicitly specified from the measurements. The calculated model corresponds to the physical model presented in the previous chapter. Comparisons between the predicted vapor fraction variety that change with thermodynamic quality are in the following section.

Figure 2 shows the calculated cross sectional averaged void fraction changed over thermodynamic quality for pressure between 7 and 15MPa. The onset of nucleate boiling (ONB) is accurately predicted, also Close agreement can be obtained from the comparison both for the trend and the trend of void fraction distribution along the whole test section is conformable with measurements.

Figure 3 shows the influence of pressure at constant heat flux Q=1.1MW·m^{-2}and mass velocity G=1000kg·m^{-2}·s^{-1}. The numerical results show well agreement with measurements, while a better agreement can be observed at a higher mass velocity, as **Figure** 2 shows. For example, an obvious deviation was found at 15MPa under a lower mass velocity 1000kg·m^{-2}·s^{-1}.

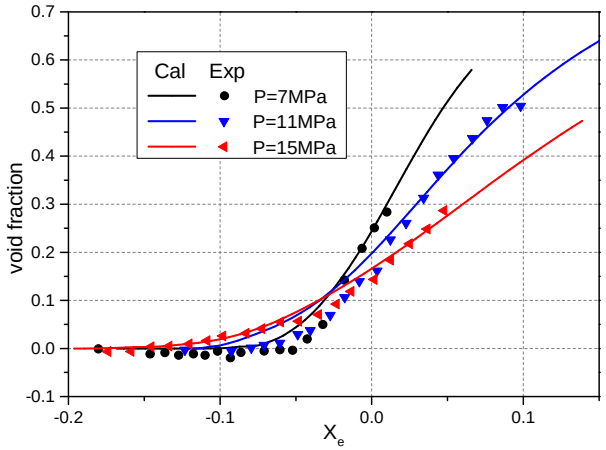

Figure 2 Q=1.1MW·m^{-2},G=2000kg·m^{-2}·s^{-1}

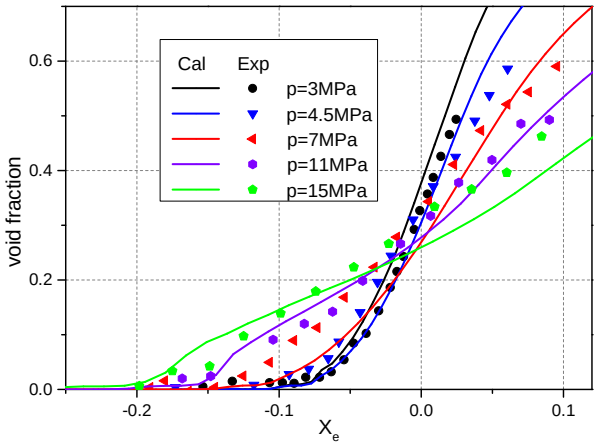

Figure 3 Q=1.1MW·m^{-2},G=1000kg·m^{-2}·s^{-1}

Mass velocity influence at certain pressure and heat flux is present **Figure** 4 and **Figure** 5. A good agreement between calculated results and experiments can be easily figured from both figure, whereas the cross sectional averaged void fraction was significantly under-estimated for the lowest mass velocity.

The impact of heat flux at constant pressure and mass velocity is illustrated in **Figure** 6 and **Figure** 7. A qualitative trend shows good agreement with measurements, whereas some quantitative errors were also found for these cases. It can be seen from **Figure** 6, the value is over-estimated at lower heat flux of 0.42 and 0.77MW·m^{-2}, and the deviation has the minimum value at high heat flux (1.72 and 2.21 MW·m^{-2}). In **Figure** 7, large discrepancy occur in cases with heat flux value of 1.13 and 1.70 MW·m^{-2}.

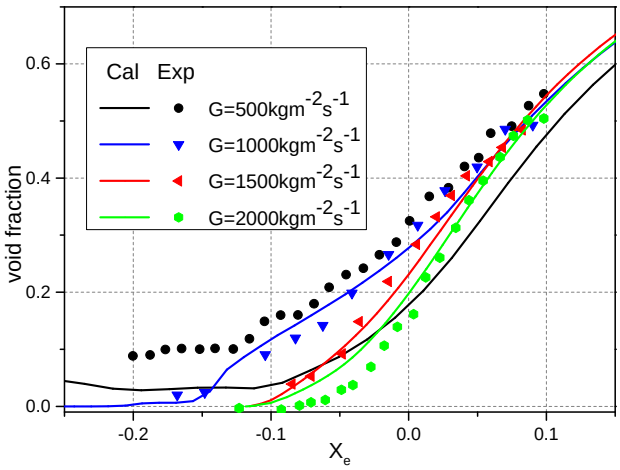

Figure 4 P=11MPa,Q=1.1MW·m^{-2}

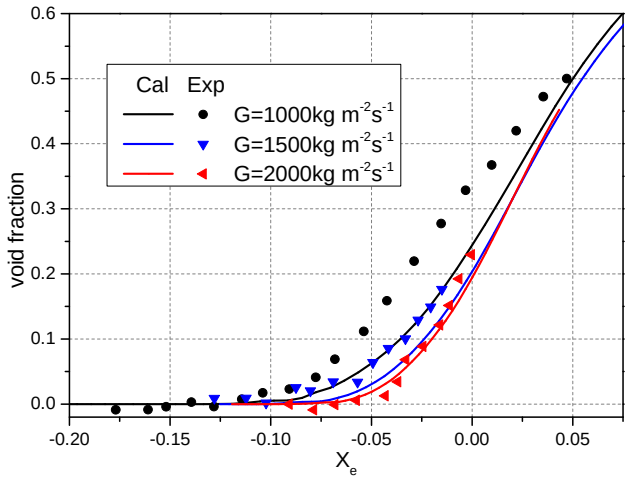

Figure 5 P=7MPa, Q=0.8MW·m^{-2}

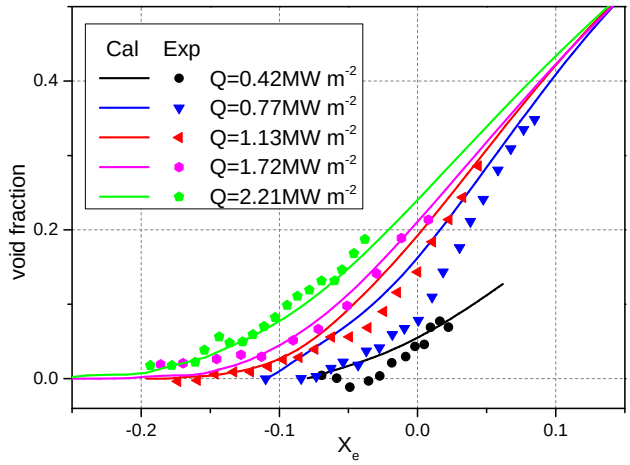

Figure 6 P=15MPa,G=2000kg·m^{-2}·s^{-1}

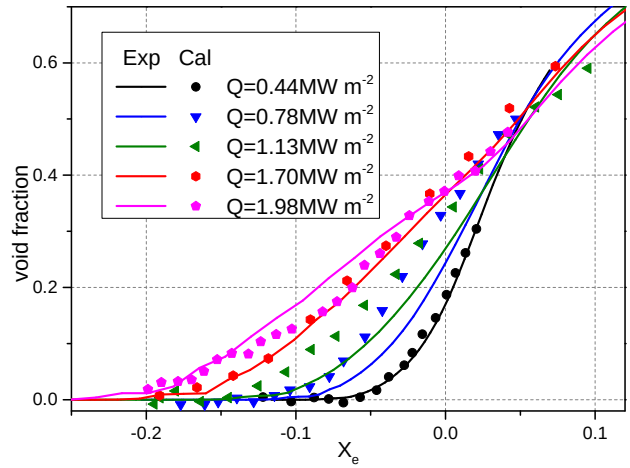

Figure 7 P=7MPa,G=1000kg·m^{-2}·s^{-1}

4. CHF PREDICTION

The benchmark data of this work were obtained from CHF experiment in vertical upward-flow pipe published by Celata[1]. In Celata et al's work, stainless steel tubes of 2.5 mm inner diameter and 100 mm length were employed to find the CHF in subcooled flow boiling with extremely high heat flux. To simplify the calculation, a quarter of the test pipe was selected as the calculated domain. The schematic diagrams of geometry and boundary conditions are given in **Figure** 8. After checking the grid independence by using four sets of grid containing 12,000, 26,400, 39,000 and 57,600 meshes respectively, we employ the grid scheme with 39,000 meshes as the grid independent grid for further calculation. The near wall cell Y+ for all the calculation based on this grid located in the range of 28.3-63.6.

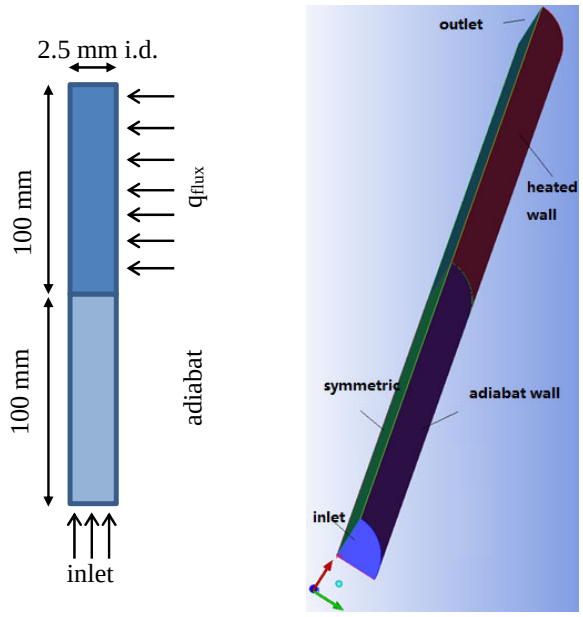

(a) geometry and corresponding boundary conditions (b) grid

Figure 8 geometry, boundary and grid

Similar to the experimental procedure, we increased the wall heat flux at heated wall by step of 0.5 MW/m2 at first and then changed the step to 0.1 MW/m2 after the CHF was approached (70% of the CHF estimated by Gunther correlation). Wall temperature increased with increasing the heat flux by little temperature step at first, and then it jumped dramatically when DNB occurred. A typical curve of maximum wall temperature with iteration was shown in **Figure** 9. As can be seen, heat flux of 0.5 MW/m^2 was set at the initial phase of calculation; after convergence (300 iterations for each heat flux step), wall heat flux was increased by 0.5 or 0.1 MW/m^2 till the DNB phenomena were detected. The wall temperature distributions along the axial direction before and after DNB were given in **Figure** 10. As can be noted, wall temperature ascended gradually when the heat flux was low than CHF; however, when the heat flux reached CHF, wall temperature shot up rapidly at a certain point where DNB occurred.

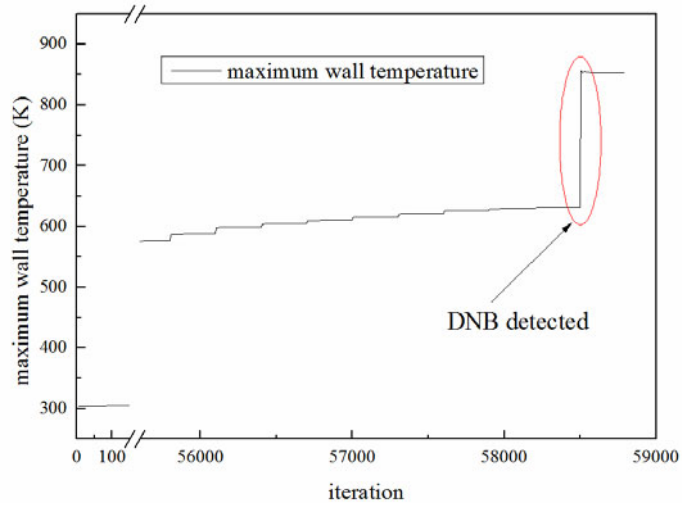

Figure 9 Maximum wall temperature with increasing wall heat flux

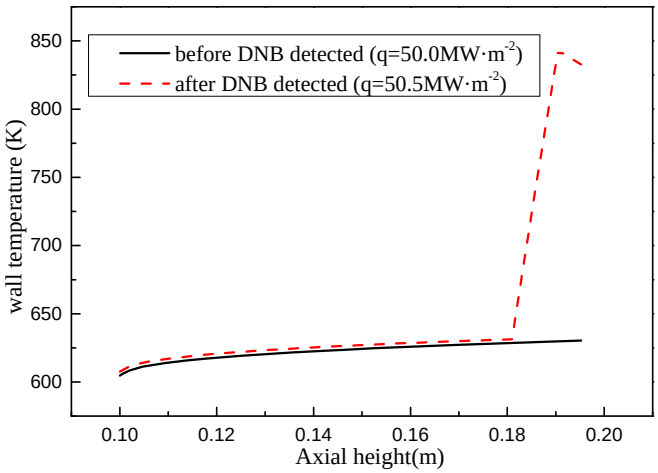

Figure 10 wall temperature along the axial direction

Figure 11 shows the three-dimensional void fraction distribution when DNB is detected. It can be noted that the maximum value occurs at the near wall region, while the minimun is on the center line of the pipe. It indicates that the flow pattern is the so called bubble flow instead of annular flow. The critical boiling type refers to departure from boiling (DNB) which represents the heat transfer limit causing a sudden increase in the wall temperature since more bubble is generated in the heated wall, rather than Dryout (DO).

We calculated 26 sets of Celata et al's experimental data and obtained the corresponding CHF data. The comparison of calculated CHF data with experimental data was given in **Figure** 12. As shown in this figure, the predicted results agreed quite well with experimental ones with deviations less than 15.0%. The mean absolute relative error of the calculated CHF (estimated by $\frac{1}{N}\sum_{i=1}^{N}\left|\frac{CHF_{exp,i}-CHF_{cal,i}}{CHF_{exp,i}}\right|$) was 7.1%.

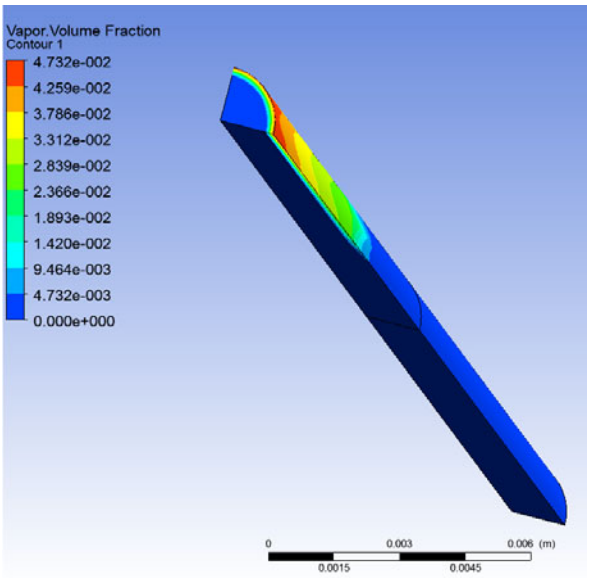

Figure 11 Three-dimensional distribution of void fraction

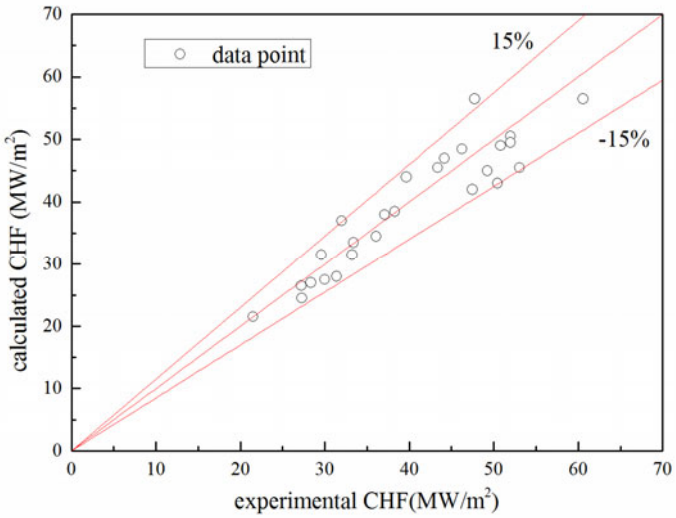

Figure 12 comparison of calculated CHF with experimental CHF

Past studies most focus on experiment, which is limited by the test section and test condition. The achievement of these work often result in CHF correlation which could not be applied to more broad applications. Wright[15] summarized the previous CHF correlations, some are listed in **Table** 1. A comparison of the empirical correlations listed in **Table** 1 with calculated results based on CFD method are shown in **Figure** 13. The results from comparison indicate that all these correlations could not predict perfectly than this study.

Figure 14 shows the effects of heated length-to-diameter ratio on CHF for a constant diameter of 2.5mm. A broad range of length-to-diameter ratio is shown, from 20 to 200, the corresponding heated length is in the range of 50 to 500. **Figure** 14 shows a fairly linear decrease in CHF with increasing length-to-diameter ratio. The more heat is transferred from heated wall to liquid with a large value of length-to-diameter, other things being equal. That could motivate more bubbles generating on the heated wall, and contribute to sharp increase in temperature.

Table 1 Previous CHF correlations

source	correlation
Oh and Englert	$\left(\frac{A_h}{A}\right)q^* = 0.458\left[1+\frac{\Delta h}{h_{fg}}\right]G^* + 2.412$
Lowdermilk et al.	$\left(\frac{A_h}{A}\right)q^* = \frac{1080}{h_{fg}D_{hy}^{0.2}}\left(\frac{4A}{A_h}\right)^{-0.15}(G)^{-0.15}G^*$
Katto	$\left(\frac{A_h}{A}\right)q^* = \left(W_L^{-1}\right)^{0.043}\left[1+11.043\left(W_L^{-1}\right)^{-0.043}\frac{\Delta h}{h_{fg}}\right]G^*, \quad W_L^{-1} = \frac{\sigma\rho_f}{G^2L}$
Mishima and Ishii	$\left(\frac{A_h}{A}\right)q^* = \frac{\Delta h_i}{h_{fg}}G^* + 2\left(\frac{1}{1.35-0.35(\rho_g/\rho_f)^{0.5}}-0.11\right)\left(\frac{s}{\lambda}\right)^{0.5}$
Monde et al.	$\left(\frac{A_h}{A}\right)q^* = \frac{0.16}{1+0.00067(\rho_f/\rho_g)^{0.6}}$

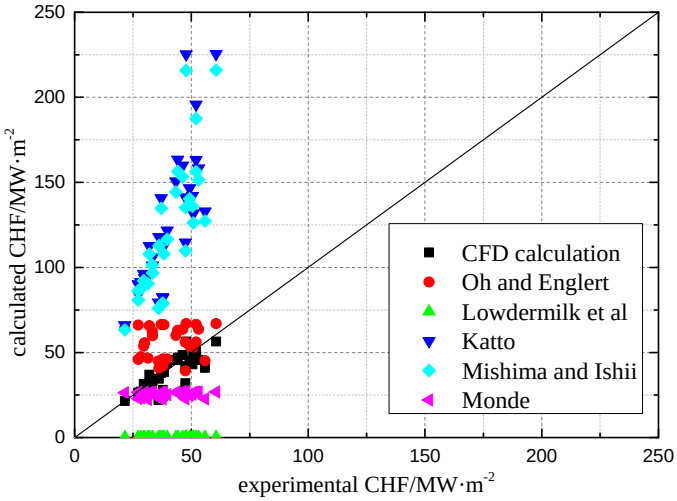

Figure 13 Comparison with empirical correlation

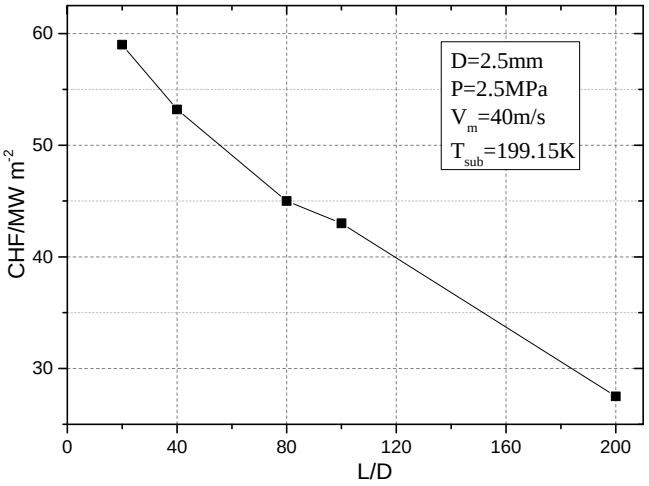

Figure 14 Effect of length-to-diameter ratio on CHF

The effect of inlet subcooling is illustrated in **Figure** 15 for inlet velocity of 20m/s and 40m/s. The cases illustrated are for a broad inlet subcooling varying from 120K to 220K. CHF increases with an increase in inlet subcooling. The growth ratio of CHF in high undercooling is larger than that in low subcooling.

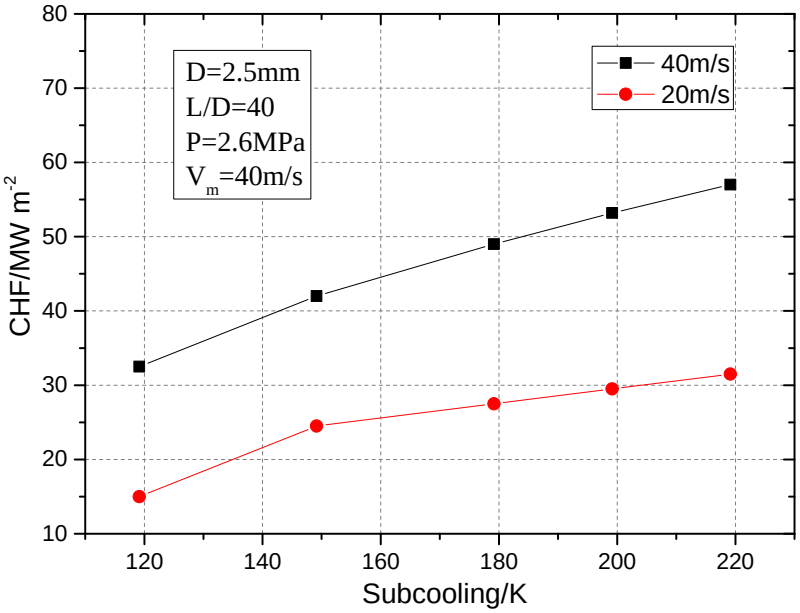

Figure 15 Effect of inlet subcooling on CHF

The effect of inlet velocity for constant value of diameter, pressure, length-to-diameter ratio and inlet subcooling is present in **Figure** 16. The inlet velocity varies from 20m/s to 50m/s. It can be easily seen that CHF is proportional to the inlet subcooling, other things being equal.

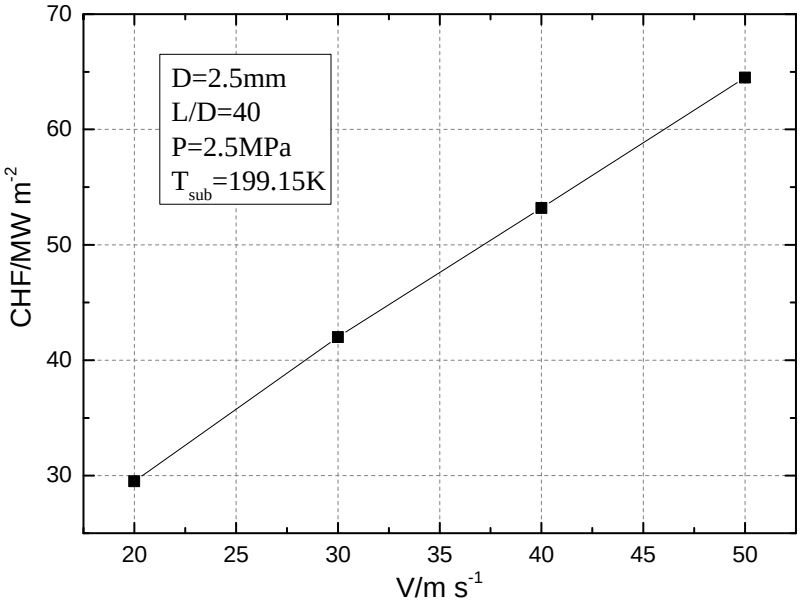

Figure 16 Effect of velocity on CHF

Figure 17 shows the variation of CHF on pressure at the existence of the heated length. Extensive numerical simulations of CHF prediction for a constant inlet subcooling are performed over a broad pressure range of 2.5MPa to 15MPa. Actually, the effect of pressure could not be isolated from inlet temperature for a fixed subcooling is given at the inlet. The inlet temperature increases with increasing pressure at a constant inlet subcooling. The CHF

increases with increasing pressure at the region from 2.5MPa to 10MPa, while the growth rate decreases with the increase in pressure. When pressure is up to 10MPa, little change can be observed with increasing pressure.

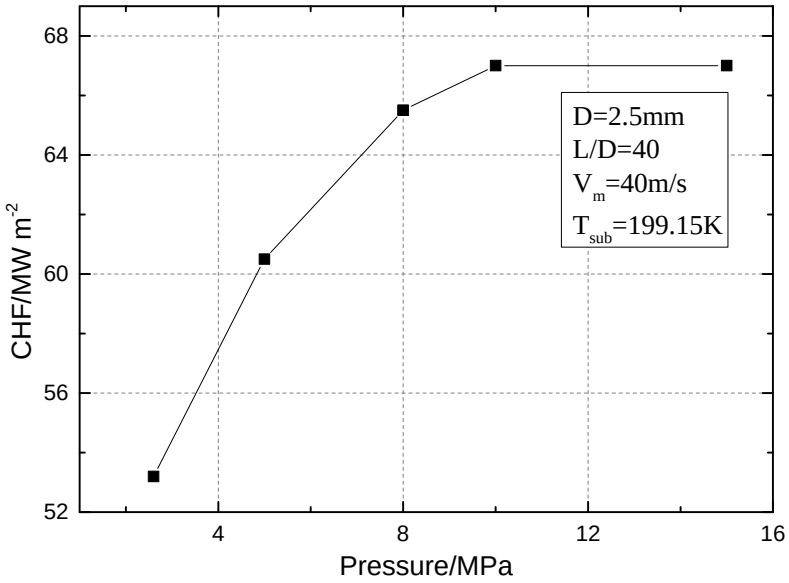

Figure 17 Effect of outlet pressure on CHF

5. CONCLUSION

In this study, RPI wall boiling model was utilized to analysis subcooled boiling phenomenon in a single pipe under both high pressure and low pressure. Afterwards CHF model developed from RPI wall boiling model was employed to investigate the DNB phenomena and predict CHF in vertical pipe. The local flow parameters can be obtained. By comparison with the corresponding experiments, the following conclusions can be drawn.

1. RPI wall boiling model can be widely applied for simulating subcooled boiling phenomenon, including the larger range of pressure, mass flow and heat flux.

2. The method proposed in this paper to predict CHF has been compared with experiment data, and is proved to be qualified to predicte CHF. Moreover, the parameter effects on CHF are also analyzed.

REFERENCE

[1] G.P. Celata, M. Cumo, A. Mariani, "Burnout in highly subcooled water flow boiling in small diameter tubes", *International Journal of Heat and Mass Transfer*, **36**(5), pp. 1269-1285 (1993).

[2] N. Kurul, M. Podowski, "On the modeling of multidimensional effects in boiling channels", *ANS Proc. 27th National Heat Transfer Conference, Minneapolis, MN*, pp. 28-31 (1991).

[3] V. Tolubinsky, D. Kostanchuk, "Vapour bubbles growth rate and heat transfer intensity at subcooled water boiling", *Heat transfer*, pp. 1-5 (1970).

[4] V.H. Del Valle, D. Kenning, "Subcooled flow boiling at high heat flux", *International Journal of Heat and Mass Transfer*, **28**(10), pp. 1907-1920 (1985).

[5] M. Lemmert, J. Chawla, "Influence of flow velocity on surface boiling heat transfer coefficient", *Heat Transfer in Boiling*, **237**(pp. 247 (1977).

[6] R. Cole, "A photographic study of pool boiling in the region of the critical heat flux", *AIChE Journal*, **6**(4), pp. 533-538 (1960).

[7] A. Ioilev, M. Samigulin, V. Ustinenko, P. Kucherova, A. Tentner, S. Lo, A. Splawski, "Advances in the modeling of cladding heat transfer and critical heat flux in boiling water reactor fuel assemblies", *Proc. 12th International Topical Meeting on Nuclear Reactor Thermal Hydraulics (NURETH-12), Pittsburgh, Pennsylvania, USA*, pp. (2007).

[8] J. Laviéville, E. Quemerais, S. Mimouni, M. Boucker, N. Mechitoua, NEPTUNE CFD V1. 0 theory manual, in, EDF, France, 2005.

[9] W. Ranz, W. Marshall, "Evaporation from drops", *Chem. Eng. Prog*, **48**(3), pp. 141-146 (1952).

[10] M. Ishii, "Two-fluid model for two-phase flow", *Multiphase Science and Technology*, **5**(1-4), pp. (1990).

[11] F. Moraga, F. Bonetto, R. Lahey, "Lateral forces on spheres in turbulent uniform shear flow", *International journal of multiphase flow*, **25**(6), pp. 1321-1372 (1999).

[12] S. Antal, R. Lahey Jr, J. Flaherty, "Analysis of phase distribution in fully developed laminar bubbly two-phase flow", *International Journal of Multiphase Flow*, **17**(5), pp. 635-652 (1991).

[13] A.D. Burns, T. Frank, I. Hamill, J.-M. Shi, "The Favre averaged drag model for turbulent dispersion in Eulerian multi-phase flows", *5th international conference on multiphase flow, ICMF*, 4, pp. (2004).

[14] G.G. Bartolemei, V.G. Brantov, Y.S. Molochnikov, Y.V. Kharitonov, V.A. Solodikk, G.N. Batashove, V.N. Mikhailov, "An experimental investigation of true volumetric vapor content with subcooled boiling in tubes", *Thermal Engineering*, **29**(3), pp. 132-135 (1982).

[15] C.T. Wright, J.E. O'Brien, R.E. Spall, "A new critical heat flux correlation for vertical water flow through multiple thin rectangular channels", *International Journal of Heat and Mass Transfer*, **51**(5-6), pp. 1071-1084 (2008).